PAPER

Composition–solubility–structure relationships in calcium (alkali) aluminosilicate hydrate (C-(N,K-)A-S-H)†

Rupert J. Myers,[a,b] Emilie L'Hôpital,[b] John L. Provis[a] and Barbara Lothenbach*[b]

The interplay between the solubility, structure and chemical composition of calcium (alkali) alumino-silicate hydrate (C-(N,K-)A-S-H) equilibrated at 50 °C is investigated in this paper. The tobermorite-like C-(N,K-)A-S-H products are more crystalline in the presence of alkalis, and generally have larger basal spacings at lower Ca/Si ratios. Both Na and K are incorporated into the interlayer space of the C-(N,K-)A-S-H phases, with more alkali uptake observed at higher alkali and lower Ca content. No relationship between Al and alkali uptake is identified at the Al concentrations investigated (Al/Si ≤ 0.1). More stable C-(N,K-)A-S-H is formed at higher alkali content, but this factor is only significant in some samples with Ca/Si ratios ≤1. Shorter chain lengths are formed at higher alkali and Ca content, and cross-linking between (alumino)-silicate chains in the tobermorite-like structure is greatly promoted by increasing alkali and Al concentrations. The calculated solubility products do not depend greatly on the mean chain length in C-(N,K-)A-S-H at a constant Ca/(Al + Si) ratio, or the Al/Si ratio in C-(N,K-)A-S-H. These results are important for understanding the chemical stability of C-(N,K-)A-S-H, which is a key phase formed in the majority of cements and concretes used worldwide.

1. Introduction

The alkali concentration in cement-based materials varies greatly as a function of the cement formulation and type: Portland cement (PC) typically contains up to 1 wt% alkali (mainly K) oxide equivalent;[1] fly ash, a common supplementary cementitious material (SCM), generally contains >1 wt% alkali (Na + K) oxide equivalent;[2] and alkali-activated cementitious materials typically involve the use of highly concentrated Na-based solutions (up to or exceeding 5 M).[3] The elevated pH

environment that prevails in hydrated cement-based materials (pH > 13) provides the crucial function of steel passivation in reinforced concrete. The alkali concentration in cement-based materials also plays an important role in the dissolution of cementitious precursors,[4,5] deterioration of concrete due to alkali–silica reactions,[6,7] and in modifying the chemical composition, structure and solubility of reaction products formed during setting and hardening.[8–11]

The main reaction product in hydrated Portland cement (PC) materials is calcium (alkali) silicate hydrate (C-(N,K-)S-H‡) with a structure analogous to the natural mineral tobermorite, usually with Ca/(Al + Si) ≥ 1.5, and sometimes with minor Al substitution up to an Al/Si ratio not exceeding 0.1.[12] This phase contains silicate (or aluminosilicate if Al is present) chains in dreierketten type arrangements, flanked on either side by a Ca–O sheet and an interlayer region (Fig. 1).[13] These aluminosilicate chains can cross-link to form Q³-type structures,[14] and if present, Al is bound in bridging sites with a strong preference over the paired sites.[15] Al is also thought to be incorporated in C-(N,K-)A-S-H in five- and six-fold coordination, *e.g.* in the interlayer (Fig. 1), although no consensus

[a]Department of Materials Science and Engineering, University of Sheffield, S1 3JD, Sheffield, UK. E-mail: rupert.myers@gmail.com, j.provis@sheffield.ac.uk
[b]Laboratory for Concrete and Construction Chemistry, EMPA, Dübendorf, 8600, Switzerland. E-mail: lhopital.emilie@gmail.com, Barbara.Lothenbach@empa.ch

‡Na and K are included in this abbreviation because these are typically the most concentrated alkali elements in cement-based materials. Cement chemistry notation is also used throughout the paper: C═CaO; S═SiO₂; A═Al₂O₃; N═Na₂O; K═K₂O; and H═H₂O.
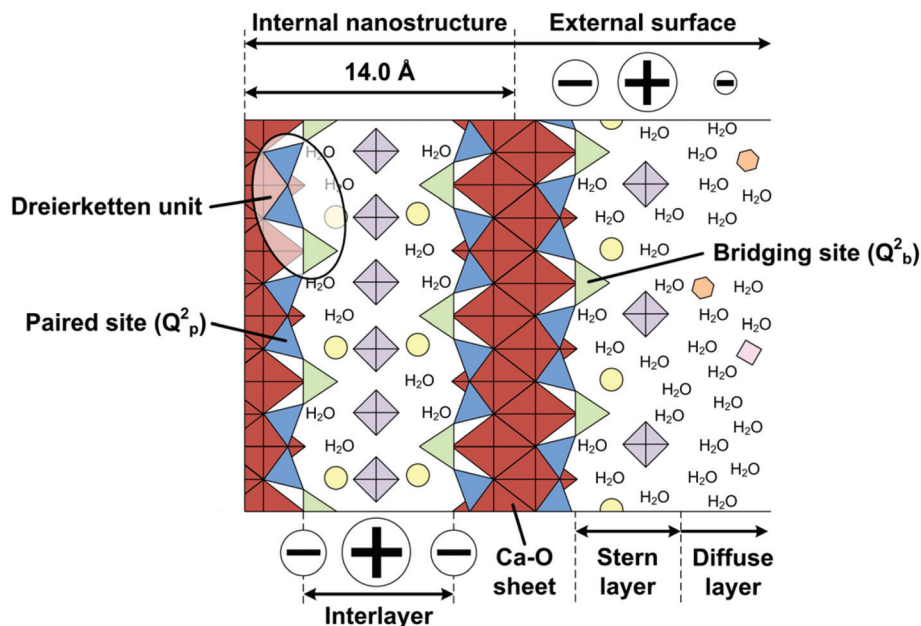
Fig. 1 Schematic representation of infinite chain length non-cross-linked C-(N,K-)A-S-H as a structural analogue of 14 Å tobermorite,[20] with stacked layers to show alkali species adsorbed on the external surface and in the interlayer region of this phase. The red diamonds are CaO polyhedra in the Ca–O sheet, and the blue and green triangles are tetrahedral aluminate or silicate units in paired and bridging sites respectively, within the dreierketten chains. The yellow circles and large purple squares represent positively-charged species that charge-neutralise the bridging sites and the rest of the layered structure respectively (typically H^+, Ca^{2+}, alkali cations such as K^+ or Na^+, and/or dissolved aluminium). The orange hexagons are diffuse layer anions (e.g. OH^- and Cl^-) that compensate the excess positive charge supplied by adsorbed cations.[19] The small pink square is an additional diffuse layer cation (e.g. Ca^{2+}, Na^+). The positive and negative symbols represent the local distribution of charge in the structure. The size, number and location of the symbols are schematic rather than crystallographically exact, and different types of hydrated alkali complexes are not distinguished.

exists regarding the location of octahedral Al in this phase.[16–18] The Ca–O sheets, interlayer regions and (alumino)-silicate chains are thought to stack together such that the chain structures form the external surfaces.[19]

The essentially aluminium-free C-(N,K-)S-H formed during plain Portland cement hydration can incorporate a significant content of alkalis (up to 20% of the amount of Na or K added[21]), which decreases as a direct function of the Ca/Si ratio.[21] A good understanding of C-(N,K-)S-H solubility currently exists up to bulk Na concentrations of 0.8 M NaOH,[8,9,21–24] which represents the pH range relevant to most cement-based materials (pH ≤ 13.5), but fewer solubility data for this phase are available for K-containing materials in the corresponding composition range.[21,22,25,26] These data are essential in understanding the long-term stability of C-(N,K-)-S-H and in the development of thermodynamic models for this phase, enabling simulation of the chemistry of cement-based materials in service.[27,28]

However, many modern blended cements contain more Al and less Ca than plain PC. The main hydrate in binders produced from these materials is a calcium (alkali) alumino-silicate hydrate (C-(N,K-)A-S-H§) with typical molar ratios of

Ca/(Al + Si) ≤ 1.5 and Al/Si > 0.1.[29,30] C-(N,K-)A-S-H phases are also major reaction products in ~2000 year old Roman cements.[31] Incorporation of alkali species into the interlayer region and on external surfaces of C-(N,K-)A-S-H is believed to occur via a charge-compensation mechanism (Fig. 1),[11,19,32,33] with less associated alkalis at higher Ca/Si ratios (similar to C-(N,K-)S-H),[34] although no consensus exists regarding the exact mechanism of alkali uptake in this phase. This is corroborated by the large variation in existing results reported for Na and K uptake as a function of Al content in C-(N,K-)A-S-H: direct correlations,[33,34] an inverse correlation,[25] and independent relationships[6,11,35] between these two parameters have been reported. There is also a lack of consensus on the selectivity of C-(N,K-)A-S-H structures between Na or K species, with existing publications reporting either no significant difference between uptake of these two alkali types,[8,21,25,34] or some degree of selectivity for K over Na.[11] This clearly demonstrates a need for additional studies to clarify the relationships between the uptake of Na, K and Al in C-(N,K-)A-S-H.

The solubility of Al-containing C-(N,K-)A-S-H is poorly understood relative to that of C-(N,K-)S-H, although recent results[14] indicate that the solubilities of these phases do not differ significantly in the absence of alkali. The availability of a comprehensive set of solubility data for C-(N,K-)A-S-H is necessary for the development of more accurate thermodynamic models for this phase,[28] which would advance the

---

§ This notation includes products with and without Al (i.e. C-(N,K-)S-H), although effort is made to distinguish these phases in the text.

utility of thermodynamic modelling in the description and performance prediction of cement-based materials. Therefore, this paper aims to clarify the effects of Na, K, Al and Ca on the chemical composition, structure, and solubility of C-(N,K-)A-S-H, utilising a dataset for C-(N,K-)A-S-H equilibrated at 50 °C. The results presented are particularly relevant for cements used for construction in large structures which experience a significant semi-adiabatic temperature rise during hydration (*e.g.* dams or foundations), or in warm climates. The results are also discussed with respect to existing solubility data at ambient conditions.

2. Materials and methods

2.1 C-(N,K-)A-S-H synthesis

C-(N,K-)A-S-H samples were synthesised at bulk molar Al/Si ratios (Al/Si*) of 0 to 0.1 and bulk molar Ca/Si ratios (Ca/Si*) of 0.6 to 1.6 using Milli-Q water (Merck Millipore) and 0 to 1 M solutions of NaOH and/or KOH (Merck Millipore), at a solution/solid ratio of 45 in a N_2-filled glovebox by the method described in ref. 8 and 14. Samples were equilibrated at 50 °C in polyethylene vessels and shaken twice per week, then filtered in a N_2-filled glovebox 56 days after synthesis, and freeze-dried for a week. Freeze-dried solids were stored in N_2-filled desiccators at ~30% relative humidity (over saturated $CaCl_2$ solutions) until analysis.

2.2 Experimental characterisation techniques

A Dionex DP ICS-3000 ion chromatograph was used to determine Ca, Si, Al, Na and K concentrations in the filtrates (relative measurement error ±10% in the concentration range of interest). Aqueous hydroxide concentrations were determined at ~24 °C with a Knick pH meter (pH-Meter 766) and a Knick SE100 electrode, which was calibrated against KOH or NaOH solutions of known concentrations. Thermogravimetric analysis (TGA) was performed using a Mettler Toledo TGA/SDTA851^e at a heating rate of 20 °C min^{-1} under an N_2 atmosphere, and derivative thermograms were calculated numerically. Powder XRD patterns were recorded on a PANalytical

lations to determine chemical compositions of the C-(N,K-)A-S-H products formed.

Solid-state ^{29}Si magic angle spinning nuclear magnetic resonance (MAS NMR) spectra were collected for the Al-free and Al/Si* = 0.1 samples synthesised with water, with 0.5 M NaOH, and with 0.5 M NaOH and 0.5 M KOH (denoted 0.5 M NaOH/0.5 M KOH) at 79.49 MHz on a Bruker Avance 400 MHz NMR spectrometer with a 7 mm CP/MAS probe. The measurements were recorded using a 4500 Hz spinning rate, 9216 scans, π/3 pulses of 2.5 μs, and a 20 s relaxation delay. ^{29}Si chemical shifts were referenced to external tetramethylsilane. Spectral deconvolutions were carried out using component peaks with a Lorentzian/Gaussian ratio of 0.5, full width at half height ≤3 ppm, and peak amplitudes constrained to be consistent with the tobermorite-like structures present in C-(N,K-)A-S-H (Appendix S1, ESI†).[37] The percentages of Al in the cross-linked components (Al$_{[C]}$) of the C-(N,K-)A-S-H products formed here are calculated using the 'Cross-linked Substituted Tobermorite Model' (CSTM) (eqn (1)):[37]

$$Al_{[C]} = 100 \frac{(Al/Si)_{[C]} \left[Q^1 + Q^2(1Al) + Q^2 + Q^3(1Al) + Q^3 \right]_{[C]}}{\sum_k \left((Al/Si)_k \left[Q^1 + Q^2(1Al) + Q^2 + Q^3(1Al) + Q^3 \right]_k \right)} \quad (1)$$

where the cross-linked and non-cross-linked components of C-(N,K-)A-S-H are represented by subscripts [C] and [NC] respectively, $k \in \{[N],[NC]\}$ and the Al/Si fractions in this formula are calculated according to eqn (2) and (3):

$$(Al/Si)_{[C]} = \frac{Q^3(1Al)}{Q^1 + Q^2 + Q^2(1Al) + Q^3 + Q^3(1Al)} \quad (2)$$

$$(Al/Si)_{[NC]} = \frac{\left(\frac{1}{2}\right)Q^2(1Al)}{Q^1 + Q^2 + Q^2(1Al)} \quad (3)$$

These parameters are used directly in eqn (4) to calculate overall Al/Si ratios of the C-(N,K-)A-S-H products formed here; this correctly describes the composition of mixed cross-linked/non-cross-linked C-(N,K-)A-S-H according to the CSTM formulation:[37]

$$(Al/Si)_{\text{C-(N,K-)A-S-H}} = \frac{\left[\frac{(Al/Si)_{[NC]}}{\left(1 + (Al/Si)_{[NC]}\right)}\right](Al+Si)_{[NC]} + \left[\frac{(Al/Si)_{[C]}}{\left(1 + (Al/Si)_{[C]}\right)}\right](Al+Si)_{[C]}}{\left[\frac{1}{\left(1 + (Al/Si)_{[NC]}\right)}\right](Al+Si)_{[NC]} + \left[\frac{1}{\left(1 + (Al/Si)_{[C]}\right)}\right](Al+Si)_{[C]}} \quad (4)$$

X'Pert Pro MDF diffractometer using a Ge(111) Johansson monochromator for Cu Kα radiation, an X'Celerator detector, and a step size of 0.017° 2θ. An external CaF_2 standard was used for Rietveld analysis to quantify of the amount of crystalline phases in each sample.[36] The ion chromatography (IC) and pH measurements, initial synthesis conditions, and solid phase assemblages and water content as determined by TGA, XRD and Rietveld analysis, were used in mass balance calcu-
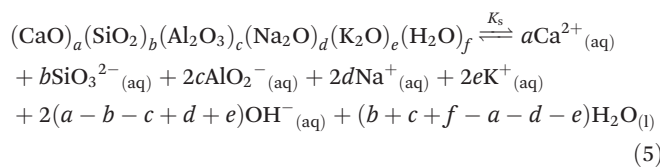
where (Al + Si) indicates the total amount of Al and Si in a C-(N,K-)A-S-H component ([C] or [NC]).

2.3 Thermodynamic modelling

Thermodynamic modelling was performed in the GEM Selektor v.3 software (http://gems.web.psi.ch/)[38,39] using the PSI/Nagra 12/07 thermodynamic database,[40] which is updated from[41] *via* the inclusion of two additional aqueous (alumino)-

silicate species, and the CEMDATA07 thermodynamic database[42–49] updated to include recently published data for Al(OH)$_3$, hydrogarnet and C-(N,K-)A-S-H.[28,50,51] Activity co-efficients were calculated using the extended Debye–Hückel equation (in Truesdell–Jones form) with the ion size and extended term parameter for KOH ($\dot{a}$ = 3.67 Å and b_γ = 0.123 kg mol^{-1}).[52] The thermodynamic properties of the aqueous species and solid phases used in these calculations are shown in Appendix S2 (ESI†).

Solubility products (K_s) for C-(N,K-)A-S-H were calculated from the generalised dissolution reaction shown in eqn (5):

$$(CaO)_a(SiO_2)_b(Al_2O_3)_c(Na_2O)_d(K_2O)_e(H_2O)_f \overset{K_s}{\rightleftharpoons} a Ca^{2+}{}_{(aq)}$$
$$+ b SiO_3{}^{2-}{}_{(aq)} + 2c AlO_2{}^-{}_{(aq)} + 2d Na^+{}_{(aq)} + 2e K^+{}_{(aq)}$$
$$+ 2(a - b - c + d + e)OH^-{}_{(aq)} + (b + c + f - a - d - e)H_2O_{(l)}$$
$$(5)$$

where a, b, c, d, e and f are the respective stoichiometric co-efficients for CaO, SiO$_2$, Al$_2$O$_3$, Na$_2$O, K$_2$O and H$_2$O in C-(N,K-)A-S-H. This reaction implies the following relationship for K_s (eqn (6)):

$$K_s = \left\{Ca^{2+}{}_{(aq)}\right\}^a \cdot \left\{SiO_3{}^{2-}{}_{(aq)}\right\}^b \cdot \left\{AlO_2{}^-{}_{(aq)}\right\}^{2c} \cdot \left\{Na^+{}_{(aq)}\right\}^{2d}$$
$$\cdot \left\{K^+{}_{(aq)}\right\}^{2e} \cdot \left\{OH^-{}_{(aq)}\right\}^{2(a-b-c+d+e)} \cdot \left\{H_2O_{(l)}\right\}^{(b+c+f-a-d-e)}$$
$$(6)$$

Activities of Ca$^{2+}{}_{(aq)}$, SiO$_3{}^{2-}{}_{(aq)}$, AlO$_2{}^-{}_{(aq)}$, Na$^+{}_{(aq)}$, K$^+{}_{(aq)}$, OH$^-{}_{(aq)}$ and H$_2$O$_{(l)}$ species were calculated with GEM-Selektor v.3,[38,39] using the measured concentrations of Ca, Si, Al, Na, K and OH$^-$ in the supernatants.

3.   Results and discussion

3.1   Solid phase analysis

The XRD results (Fig. 2) show that the main solid phase formed in each of the Al-free samples is C-(N,K-)S-H (phase quantification is presented as ESI, Appendix S3†). This is the only reaction product identified in the samples synthesised with Ca/Si* ratios of 0.6 and 1 by XRD and TGA (ESI, Appendix S4†). Reflections assigned to portlandite (Ca(OH)$_2$, Powder Diffraction File (PDF)# 00-044-1481) are only present in the data for the Al-free sample synthesised with 0.5 M NaOH/ 0.5 M KOH at a Ca/Si* ratio of 1.4, although portlandite is also identified in some other Al-free samples synthesised with alkali hydroxide solutions and Ca/Si* ratios ≥1.2. Portlandite has been observed in C-(N,K-)S-H samples cured for 3 weeks or longer at 25 °C with Ca/Si* ratios >1 and [NaOH] ≥ 1 M,[9,23] in good agreement with these results. Calcite (CaCO$_3$, PDF# 00-005-0586), aragonite (CaCO$_3$, PDF# 00-041-1475), natrite (Na$_2$CO$_3$, PDF# 01-075-6816), thermonatrite (Na$_2$CO$_3$·H$_2$O, PDF# 00-005-0586) and trona (Na$_3$H(CO$_3$)$_2$·2H$_2$O, PDF# 01-078-1064) are present in some of the samples, formed by super-ficial carbonation during preparation and/or analysis.

The solid reaction products identified in the C-(N,K-)A-S-H samples with Al/Si* = 0.05 are similar to those identified in

their Al-free counterparts: the main reaction product in each specimen is C-(N,K-)A-S-H, and portlandite is only identified in samples synthesised with 0.1 M and 1 M alkali hydroxide solutions at Ca/Si* ratios ≥1.2 (Fig. 2). Katoite ((CaO)$_3$(Al$_2$O$_3$)-(H$_2$O)$_6$, PDF# 00-024-0217) is additionally present in some samples, although only in minor amounts (≤2 wt% of the total sample mass). The superficial carbonation products calcite, aragonite, vaterite (CaCO$_3$, PDF# 04-015-9018), natrite and thermonatrite are identified in some of the Al-containing samples. These phase assemblages are similar to those identi-fied by XRD in C-(N,K-)A-S-H samples synthesised using the same method and bulk chemical compositions but at 20 °C.[8] The small peaks at 12.6° 2θ and 11.3° 2θ in the diffractograms of the Ca/Si* = 0.6 and Ca/Si* = 1 samples synthesised with 0.5 M NaOH/0.5 M KOH are tentatively assigned to K-natrolite (PDF# 01-080-0519)[53] and carbonated calcium hemicarbo-aluminate hydrate (0.125 < C/Ca < 0.25),[54] respectively.

The C-(N,K-)A-S-H products in the alkali-containing samples are much more crystalline than the specimen pre-pared in the absence of alkalis, as identified by the much clearer and sharper (002) reflections between 5 and 10° 2θ in the presence of Na and/or K (Fig. 2). The effects of C-(N,K-)A-S-H chemical composition and alkali hydroxide concentration on the (002) reflections are presented in section 3.3 below.

3.2   Aqueous phase analysis

The measured concentrations of Si, Ca and OH$^-$ in the super-natants of the C-(N,K-)A-S-H samples do not change greatly as a function of the bulk Al concentration (Fig. 3). In general, the measured aqueous Si and OH$^-$ concentrations are higher and the dissolved Ca concentrations are lower in samples syn-thesised with solutions containing more alkalis. The aqueous Si concentrations typically decrease and the dissolved Ca con-centrations generally increase as functions of the Ca/Si* ratio. The OH$^-$ concentrations are generally greater and less depen-dent on chemical composition at higher bulk Ca content. These results are consistent with existing solubility measure-ments in the CaO-(Na$_2$O,K$_2$O)-Al$_2$O$_3$-SiO$_2$-H$_2$O systems at ~25 °C,[21–24,35,55,56] which show the same trends in dissolved Si, Ca and OH$^-$ concentrations with respect to the bulk alkali content and Ca/Si ratio. Here, dissolved Al concentrations were generally found to be lower at higher Ca/Si* ratios, and higher in samples more highly concentrated in alkalis.

Dissolved Si, Ca and OH$^-$ concentrations in the sample sets synthesised with 0.1 M KOH and with 0.1 M NaOH are equal for Ca/Si* ≥ 1.2, and are also similar for most samples with lower Ca content (Fig. 3). This result suggests that C-(N,K-)A-S-H solubility does not vary greatly as a function of the nature of the alkali cation (Na or K) present. However, the large changes in dissolved Si, Ca, OH$^-$ and Al concentrations as functions of the bulk alkali concentration and the Ca/Si ratio indicate that C-(N,K-)A-S-H solubility may change significantly with respect to these parameters, as will be discussed further in section 3.4. Saturation indices calculated using the measured aqueous Si, Ca, OH$^-$ and Al concentrations shown in Fig. 3 indicate that the samples containing katoite (e.g. the Ca/Si* = 1, Al/Si* =
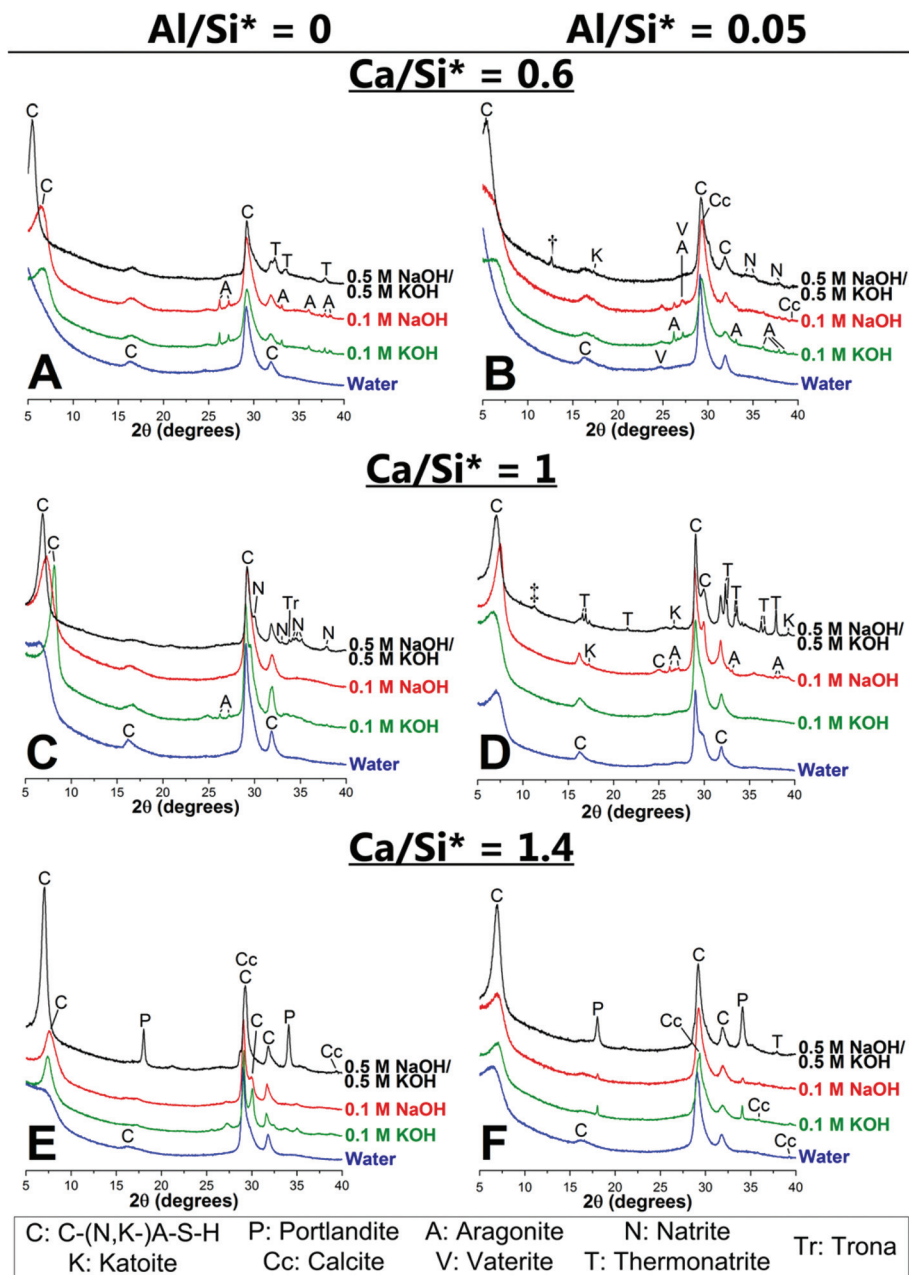
Fig. 2 Cu Kα diffractograms of C-(N,K-)A-S-H samples equilibrated at 50 °C: (A) Ca/Si* = 0.6 and Al/Si* = 0; (B) Ca/Si* = 0.6 and Al/Si* = 0.05; (C) Ca/Si* = 1 and Al/Si* = 0; (D) Ca/Si* = 1 and Al/Si* = 0.05; (E) Ca/Si* = 1.4 and Al/Si* = 0; and (F) Ca/Si* = 1.4 and Al/Si* = 0.05. The peaks marked by † and ‡ are tentatively assigned to K-natrolite and carbonated calcium hemicarboaluminate hydrate. Ca/Si* = bulk Ca/Si. Al/Si* = bulk Al/Si.

0.05, 0.5 M NaOH/0.5 M KOH sample, see Fig. 2) did not reach equilibrium within the experimental timeframe here, as this phase is calculated to be undersaturated in the systems analysed. There was otherwise good agreement between the phase assemblages formed and the calculated saturation indices. These results are presented in detail as ESI (Appendix S5†).

3.3 C-(N,K-)A-S-H chemical composition and basal spacing

Chemical compositions of the C-(N,K-)A-S-H products formed at Al/Si* ratios = 0 and 0.05 are shown in Tables 1 and 2. Most

of the C-(N,K-)A-S-H products formed at 0.6 ≤ Ca/Si* ratios ≤1.4 have Ca/Si and Al/Si ratios similar to the bulk synthesis conditions used in the samples synthesised with water and 0.1 M alkali solutions, due to the relatively low levels of secondary or superficial carbonation products formed in these specimen (yield is ≥91 wt% C-(N,K-)A-S-H in these samples; Appendix S3, ESI†). Samples synthesised with Ca/Si* ratios = 1.6 and alkali hydroxide solutions contain more portlandite due to the decreased solubility of this phase at higher Ca and alkali content (Tables 1 and 2).
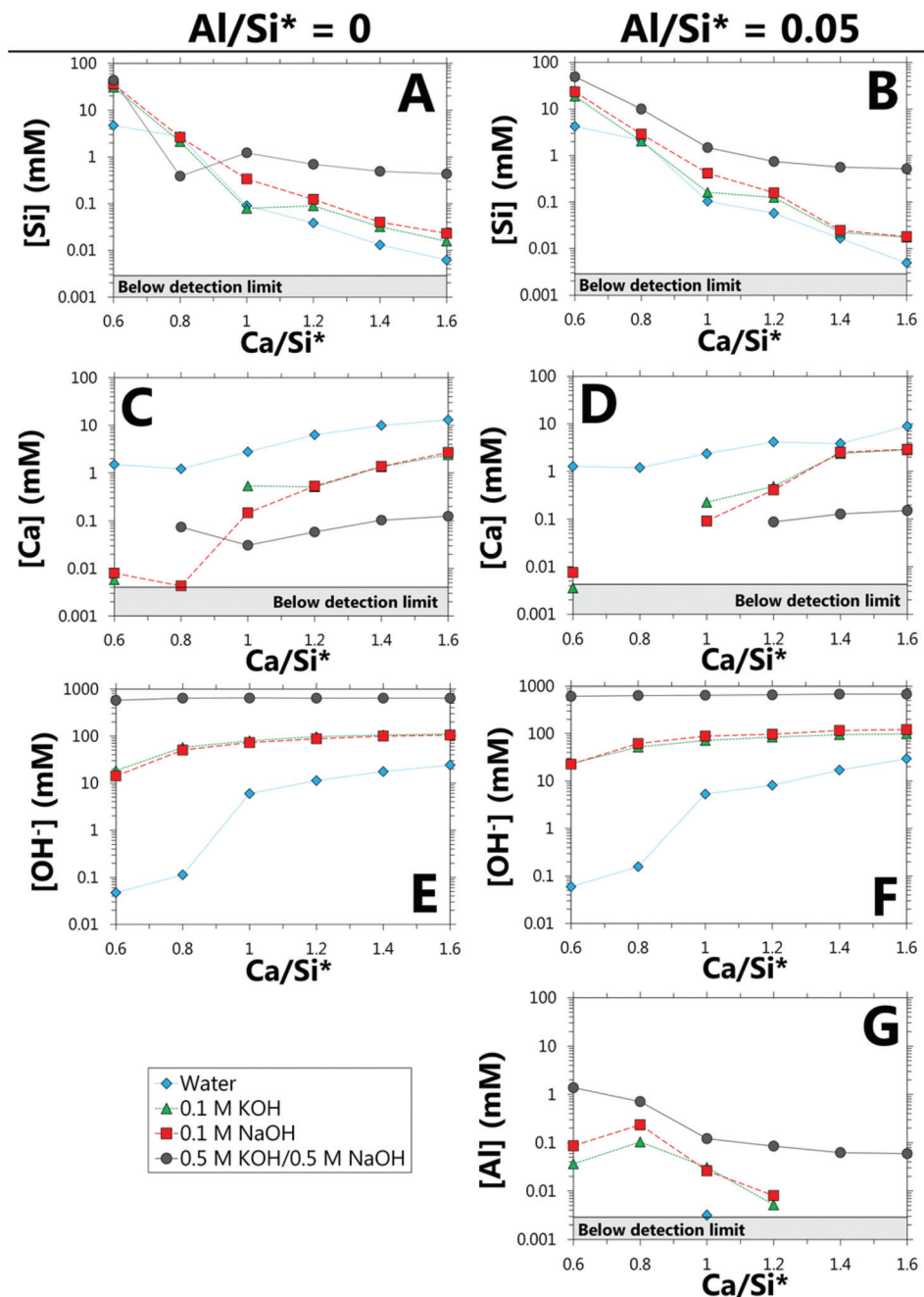
Fig. 3 Concentrations of dissolved Si, Ca, OH⁻ and Al in the supernatants of the C-(N,K-)A-S-H samples: (A) [Si], Al/Si* = 0; (B) [Si], Al/Si* = 0.05; (C) [Ca], Al/Si* = 0; (D) [Ca], Al/Si* = 0.05; (E) [OH⁻], Al/Si* = 0; (F) [OH⁻], Al/Si* = 0.05; (G) [Al], Al/Si* = 0.05. OH⁻ concentrations are calculated from pH measurements at ~24 °C. The estimated relative uncertainty of the IC measurements is ±10%. Ca/Si* = bulk Ca/Si. Al/Si* = bulk Al/Si. Lines are for eye-guides only. These results are tabulated in Appendix S6 (ESI†).

The C-(N,K-)A-S-H products typically contain $H_2O/(Al + Si)$ ratios between 1 and 2 (Fig. 4): the H_2O content in C-(N,K-)A-S-H was determined by assigning the mass losses between 30 °C and 550 °C to the decomposition of C-(N,K-)A-S-H, portlandite, katoite and $Al(OH)_3$ during heating by TGA (Appendix S4, ESI†). Portlandite was the only secondary product quantified by TGA and used in C-(N,K-)A-S-H chemical composition calculations in the absence of XRD data; the formation of only very

small quantities of other secondary products here (≤2 wt% of the total mass of each sample) means that any errors introduced into the reported C-(N,K-)A-S-H chemical compositions due to use of this method are minor.

The reported $H_2O/(Al + Si)$ ratios (Fig. 4) are in relatively good agreement with the expected result for C-(N,K-)A-S-H equilibrated at ~30% RH, where no 'free' water is present and some adsorbed water is removed,[57,58] and with the H_2O

Table 1 Chemical compositions of the C-(N,K-)S-H products (Al/Si* = 0), determined from Rietveld analysis and IC, TGA, XRD and pH measurements (normal font), and from IC, TGA and pH measurements considering C-(N,K-)S-H and portlandite only (italic font). The estimated absolute errors are ±0.05 units in the Ca/(Al + Si) ratios, ±0.2 units in the H_2O/(Al + Si) ratios, and ±0.08 units for the 0.1 M alkali samples and ±0.7 for the 1 M alkali samples in the (Na + K)/(Al + Si) ratios of the C-(N,K-)S-H products. Ca/Si* = bulk Ca/Si

Synthesis solution	C-(N,K-)S-H chemical formula	Ca/Si	Na/Si	K/Si	H_2O/Si
Ca/Si* = 0.6					
Water	$(CaO)_{0.61}(SiO_2)_1(H_2O)_{1.1}$	0.61	n/a [a]	n/a [b]	1.1
0.1 M NaOH	$(CaO)_{0.70}(Na_2O)_{0.11}(SiO_2)_1(H_2O)_{1.6}$	0.70	0.23	n/a [b]	1.6
0.1 M KOH	$(CaO)_{0.69}(K_2O)_{0.13}(SiO_2)_1(H_2O)_{1.6}$	0.69	n/a [a]	0.27	1.6
0.5 M NaOH/0.5 M KOH	$(CaO)_{0.73}(Na_2O)_{0.04}(K_2O)_{0.08}(SiO_2)_1(H_2O)_{1.7}$	0.73	0.08	0.16	1.7
Ca/Si* = 0.8					
Water	*$(CaO)_{0.80}(SiO_2)_1(H_2O)_{1.9}$*	*0.80*	*n/a [a]*	*n/a [b]*	*1.9*
0.1 M NaOH	*$(CaO)_{0.81}(Na_2O)_{0.09}(SiO_2)_1(H_2O)_{1.5}$*	*0.81*	*0.18*	*n/a [b]*	*1.5*
0.1 M KOH	*$(CaO)_{0.81}(K_2O)_{0.10}(SiO_2)_1(H_2O)_{1.3}$*	*0.81*	*n/a [a]*	*0.21*	*1.3*
0.5 M NaOH/0.5 M KOH	*$(CaO)_{0.3}(Na_2O)_{0.02}(K_2O)_{0.02}(SiO_2)_1(H_2O)_{1.1}$* [c]	*0.30* [c]	*0.03* [c]	*0.04* [c]	*1.1* [c]
Ca/Si* = 1					
Water	$(CaO)_{1.0}(SiO_2)_1(H_2O)_{1.4}$	1.0	n/a [a]	n/a [b]	1.4
0.1 M NaOH	$(CaO)_{1.0}(Na_2O)_{0.06}(SiO_2)_1(H_2O)_{1.3}$	1.0	0.12	n/a [b]	1.3
0.1 M KOH	$(CaO)_{1.0}(K_2O)_{0.07}(SiO_2)_1(H_2O)_{1.6}$	1.0	n/a [a]	0.13	1.6
0.5 M NaOH/0.5 M KOH	$(CaO)_{1.0}(Na_2O)_{0.07}(K_2O)_{0.08}(SiO_2)_1(H_2O)_{1.7}$	1.0	0.15	0.17	1.7
Ca/Si* = 1.2					
Water	*$(CaO)_{1.2}(SiO_2)_1(H_2O)_{1.5}$*	*1.2*	*n/a [a]*	*n/a [b]*	*1.5*
0.1 M NaOH	*$(CaO)_{1.2}(Na_2O)_{0.02}(SiO_2)_1(H_2O)_{1.4}$*	*1.2*	*0.05*	*n/a [b]*	*1.4*
0.1 M KOH	*$(CaO)_{1.2}(K_2O)_{0.03}(SiO_2)_1(H_2O)_{1.6}$*	*1.2*	*n/a [a]*	*0.06*	*1.6*
0.5 M NaOH/0.5 M KOH	*$(CaO)_{1.0}(Na_2O)_{0.09}(K_2O)_{0.08}(SiO_2)_1(H_2O)_{2.0}$*	*1.0*	*0.19*	*0.16*	*2.0*
Ca/Si* = 1.4					
Water	$(CaO)_{1.3}(SiO_2)_1(H_2O)_{1.9}$	1.3	n/a [a]	n/a [b]	1.9
0.1 M NaOH	$(CaO)_{1.4}(SiO_2)_1(H_2O)_{1.7}$	1.4	<0.01	n/a [b]	1.7
0.1 M KOH	$(CaO)_{1.4}(K_2O)_{0.02}(SiO_2)_1(H_2O)_{1.9}$	1.4	n/a [a]	0.03	1.9
0.5 M NaOH/0.5 M KOH	$(CaO)_{1.4}(Na_2O)_{0.09}(K_2O)_{0.08}(SiO_2)_1(H_2O)_{2.1}$	1.4	0.18	0.16	2.1
Ca/Si* = 1.6					
Water	*$(CaO)_{1.5}(SiO_2)_1(H_2O)_{2.0}$*	*1.5*	*n/a [a]*	*n/a [b]*	*2.0*
0.1 M NaOH	*$(CaO)_{1.4}(SiO_2)_1(H_2O)_{1.8}$*	*1.4*	*<0.01*	*n/a [b]*	*1.8*
0.1 M KOH	*$(CaO)_{1.4}(K_2O)_{0.01}(SiO_2)_1(H_2O)_{1.7}$*	*1.4*	*n/a [a]*	*0.02*	*1.7*
0.5 M NaOH/0.5 M KOH	*$(CaO)_{1.3}(SiO_2)_1(H_2O)_{1.1}$*	*1.3*	*<0.01*	*<0.01*	*1.1*

[a] n/a = not applicable: no Na was added during synthesis (<0.6 mM Na is present as an impurity in the 0.1 M KOH synthesis solution). [b] n/a = not applicable: no K was added during synthesis. [c] An additional major phase, possibly a zeolite, was formed in this sample in addition to C-(N,K-)S-H.

content of C-(N,K-)A-S-H synthesised at 20 °C.[8] In general, the H_2O/(Al + Si) ratios increase slightly as a direct function of the Ca/(Al + Si) ratios of the C-(N,K-)A-S-H products formed, but no significant correlations are found between the H_2O/(Al + Si) ratio and the alkali or Al content in this phase. A strong direct relationship between the H_2O/(Al + Si) and Ca/(Al + Si) ratios is reported for laboratory-synthesised C-S-H,[59] but is not as evident here from the data presented in Fig. 4. Chemical compositions of the C-(N,K-)A-S-H products synthesised using 0.5 M NaOH/0.5 KOH solutions are omitted from Fig. 4 due to the relatively higher quantities of secondary products formed in these samples.

The alkali and Al contents of the C-(N,K-)A-S-H products formed are independent of each other when relatively low amounts of Al are present (comparing the darker-coloured symbols with Al/Si* = 0 to the lighter-coloured symbols with Al/Si* = 0.05 in Fig. 5). At Al/Si* ratios ≤0.05, all of the Al added is generally incorporated into C-(N,K-)A-S-H products when synthesised with water and no added alkalis (Table 2).[14] However, the amount of Al which can be incorporated into C-(N,K-)A-S-H is related to the dissolved concentration of this element at higher bulk Al content: increasing the bulk Na or K

concentration increases the amount of dissolved Al (Fig. 3) and consequently also the amount of Al which can be incorporated into C-(N,K-)A-S-H.[8] This description is consistent with ^{29}Si MAS NMR analysis of hydrated white PC with different alkali contents,[33] which showed the formation of C-(N,K-)A-S-H products with increased Al/Si ratios at higher bulk alkali concentration. This description is also in agreement with the lack of a direct relationship found in[11] between alkali and Al content in laboratory-synthesised C-(N,K-)S-H, and in C-(N,K-)A-S-H with Al/Si = 0.04 in hydrated blends of PC and silica fume.

The amount of Na and K incorporated in the C-(N,K-)A-S-H products decreases with the Ca/(Al + Si) ratio of this phase (Fig. 5), from (Na + K)/(Al + Si) = 0.25 at Ca/(Al + Si) = 0.6 to zero Na and K incorporated at Ca/(Al + Si) = 1.6. This trend, and the quantified (Na + K)/(Al + Si) ratios, are consistent with those reported in earlier studies of alkali uptake in laboratory-synthesised C-(N,K-)A-S-H at room temperature.[21,25,34,60] The (Na + K)/(Al + Si) ratios of the C-(N,K-)A-S-H products are independent of the nature of the alkali element (Na or K).

The increased alkali uptake determined here for C-(N,K-)A-S-H with lower Ca/(Al + Si) ratios (Fig. 5) is explained in

Table 2 Chemical compositions of the C-(N,K-)A-S-H products (Al/Si* = 0.05), determined from Rietveld analysis and IC, TGA, XRD and pH measurements (normal font), and from IC, TGA and pH measurements considering C-(N,K-)S-H and portlandite only (italic font). The estimated absolute errors are ±0.05 units in the Ca/(Al + Si) ratios, ±0.2 units in the H_2O/(Al + Si) ratios, ±0.02 units in the Al/Si ratios, and ±0.08 units for the 0.1 M alkali samples and ±0.7 for the 1 M alkali samples in the (Na + K)/(Al + Si) ratios of the C-(N,K-)A-S-H products. Ca/Si* = bulk Ca/Si

Synthesis solution	C-(N,K-)A-S-H chemical formula	Ca/(Al + Si)	Al/Si	Na/(Al + Si)	K/(Al + Si)	H_2O/(Al + Si)
Ca/Si* = 0.6						
Water	$(CaO)_{0.60}(Al_2O_3)_{0.026}(SiO_2)_1(H_2O)_{1.4}$	0.57	0.051	n/a [a]	n/a [b]	1.3
0.1 M NaOH	$(CaO)_{0.66}(Al_2O_3)_{0.028}(Na_2O)_{0.13}(SiO_2)_1(H_2O)_{1.7}$	0.63	0.055	0.25	n/a [b]	1.6
0.1 M KOH	$(CaO)_{0.65}(Al_2O_3)_{0.027}(K_2O)_{0.13}(SiO_2)_1(H_2O)_{1.2}$	0.62	0.054	n/a [a]	0.24	1.1
0.5 M NaOH/0.5 M KOH	$(CaO)_{0.76}(Al_2O_3)_{0.028}(Na_2O)_{0.13}(K_2O)_{0.13}(SiO_2)_1(H_2O)_{1.9}$	0.72	0.056	0.24	0.24	1.8
Ca/Si* = 0.8						
Water	$(CaO)_{0.80}(Al_2O_3)_{0.025}(SiO_2)_1(H_2O)_{1.7}$	0.76	0.051	n/a [a]	n/a [b]	1.6
0.1 M NaOH	$(CaO)_{0.81}(Al_2O_3)_{0.025}(Na_2O)_{0.11}(SiO_2)_1(H_2O)_{1.4}$	0.77	0.050	0.21	n/a [b]	1.3
0.1 M KOH	$(CaO)_{0.81}(Al_2O_3)_{0.025}(K_2O)_{0.10}(SiO_2)_1(H_2O)_{1.2}$	0.77	0.050	n/a [a]	0.19	1.1
0.5 M NaOH/0.5 M KOH	$(CaO)_{0.84}(Al_2O_3)_{0.024}(Na_2O)_{0.18}(K_2O)_{0.17}(SiO_2)_1(H_2O)_{2.8}$	0.80	0.049	0.35	0.33	2.7
Ca/Si* = 1						
Water	$(CaO)_{0.99}(Al_2O_3)_{0.025}(SiO_2)_1(H_2O)_{1.5}$	0.94	0.050	n/a [a]	n/a [b]	1.4
0.1 M NaOH	$(CaO)_{1.0}(Al_2O_3)_{0.023}(Na_2O)_{0.06}(SiO_2)_1(H_2O)_{1.3}$	1.00	0.045	0.12	n/a [b]	1.3
0.1 M KOH	$(CaO)_{1.0}(Al_2O_3)_{0.025}(K_2O)_{0.06}(SiO_2)_1(H_2O)_{1.3}$	0.95	0.050	n/a [a]	0.11	1.3
0.5 M NaOH/0.5 M KOH	$(CaO)_{1.0}(Al_2O_3)_{0.025}(Na_2O)_{0.13}(K_2O)_{0.10}(SiO_2)_1(H_2O)_{1.8}$	0.96	0.050	0.25	0.20	1.7
Ca/Si* = 1.2						
Water	$(CaO)_{1.2}(Al_2O_3)_{0.025}(SiO_2)_1(H_2O)_{1.8}$	1.12	0.050	n/a [a]	n/a [b]	1.7
0.1 M NaOH	$(CaO)_{1.2}(Al_2O_3)_{0.025}(Na_2O)_{0.04}(SiO_2)_1(H_2O)_{1.5}$	1.14	0.050	0.08	n/a [b]	1.4
0.1 M KOH	$(CaO)_{1.2}(Al_2O_3)_{0.025}(K_2O)_{0.02}(SiO_2)_1(H_2O)_{1.4}$	1.14	0.050	n/a [a]	0.04	1.4
0.5 M NaOH/0.5 M KOH	$(CaO)_{1.0}(Al_2O_3)_{0.025}(Na_2O)_{0.14}(K_2O)_{0.10}(SiO_2)_1(H_2O)_{1.8}$	0.99	0.050	0.26	0.20	1.7
Ca/Si* = 1.4						
Water	$(CaO)_{1.4}(Al_2O_3)_{0.025}(SiO_2)_1(H_2O)_{1.9}$	1.3	0.050	n/a [a]	n/a [b]	1.8
0.1 M NaOH	$(CaO)_{1.4}(Al_2O_3)_{0.025}(Na_2O)_{0.02}(SiO_2)_1(H_2O)_{1.8}$	1.3	0.050	0.05	n/a [b]	1.8
0.1 M KOH	$(CaO)_{1.4}(Al_2O_3)_{0.025}(SiO_2)_1(H_2O)_{1.5}$	1.3	0.050	n/a [a]	<0.01	1.4
0.5 M NaOH/0.5 M KOH	$(CaO)_{1.2}(Al_2O_3)_{0.025}(Na_2O)_{0.12}(K_2O)_{0.10}(SiO_2)_1(H_2O)_{1.7}$	1.2	0.050	0.23	0.19	1.6
Ca/Si* = 1.6						
Water	$(CaO)_{1.5}(Al_2O_3)_{0.025}(SiO_2)_1(H_2O)_{2.1}$	1.5	0.050	n/a [a]	n/a [b]	2.0
0.1 M NaOH	$(CaO)_{1.3}(Al_2O_3)_{0.025}(Na_2O)_{0.02}(SiO_2)_1(H_2O)_{1.7}$	1.3	0.050	0.03	n/a [b]	1.7
0.1 M KOH	$(CaO)_{1.3}(Al_2O_3)_{0.025}(SiO_2)_1(H_2O)_{1.5}$	1.2	0.050	n/a [a]	<0.01	1.4
0.5 M NaOH/0.5 M KOH	$(CaO)_{1.2}(Al_2O_3)_{0.025}(Na_2O)_{0.15}(K_2O)_{0.12}(SiO_2)_1(H_2O)_{1.8}$	1.2	0.050	0.29	0.23	1.7

[a] n/a = not applicable: no Na was added during synthesis (<0.6 mM Na is present as an impurity in the 0.1 M KOH synthesis solution). [b] n/a = not applicable: no K was added during synthesis.
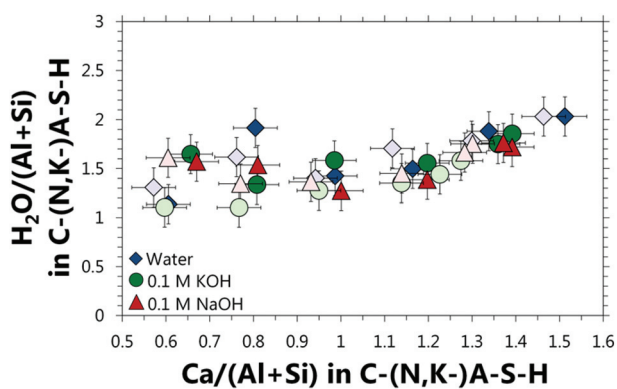
Fig. 4 H_2O/(Al + Si) ratios of the (Al/Si* = 0) C-(N,K-)S-H (dark symbols) and Al/Si* = 0.05 C-(N,K-)A-S-H (light symbols) as functions of the Ca/(Al + Si) ratio, for samples synthesised with ≤0.1 M alkali hydroxide solutions and equilibrated at 50 °C. The estimated absolute errors are ±0.05 units in the Ca/(Al + Si) ratios and ±0.2 in the H_2O/(Al + Si) ratios of the C-(N,K-)A-S-H products.
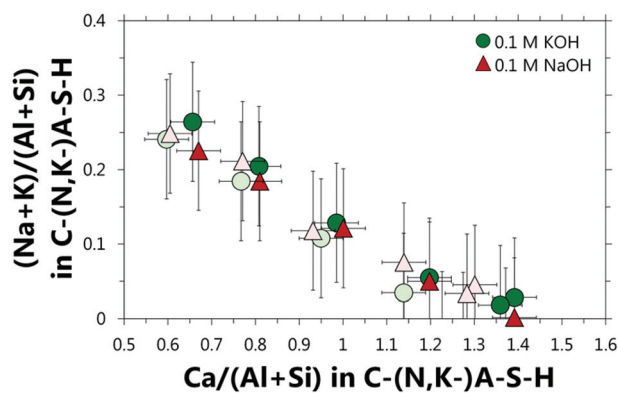
Fig. 5 Alkali cation uptake in C-(N,K-)S-H (Al/Si* = 0, dark symbols) and Al/Si* = 0.05 C-(N,K-)A-S-H (light symbols) as functions of the Ca/(Al + Si) ratio, for samples synthesised with 0.1 M alkali hydroxide solutions at 50 °C. The estimated absolute errors are ±0.05 units in the Ca/(Al + Si) ratios and ±0.08 units in the (Na + K)/(Al + Si) ratios of the C-(N,K-)A-S-H products.

terms of the incorporation of more alkali in C-(N,K-)A-S-H interlayer spaces at lower Ca content. This explanation is consistent with the largest basal spacings measured here at the

lowest Ca/(Al + Si) ratios, at a fixed alkali hydroxide concentration (Fig. 6). An inverse relationship between basal spacing and Ca/(Al + Si) ratio has also been reported for alkali-free
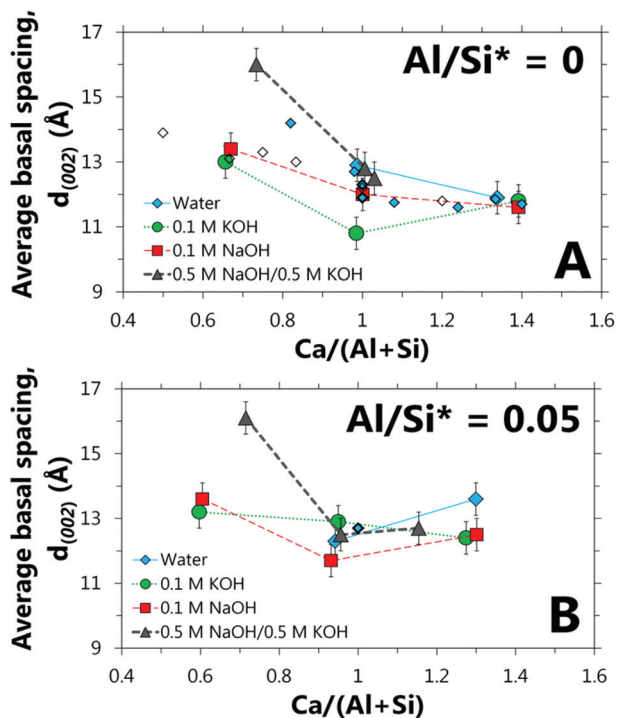
Fig. 6 Average ($d_{(002)}$) basal spacings (estimated uncertainty = ±0.5 Å) of the C-(N,K-)A-S-H products synthesised with (A) Al/Si* = 0 and (B) Al/Si* = 0.05 (large symbols). Small bold filled diamonds are data from samples equilibrated at 20 °C in ref. 8, small filled diamonds are data for 21-day old samples from ref. 62, and small open diamonds are data from ref. 63. Al/Si* represents the bulk Al/Si ratio.

calcium silicate hydrate[61] and alkali-free calcium alumino-silicate hydrate (C-A-S-H) with Ca/(Al + Si) ratios <1.[62]

The positions of the (002) reflections in Fig. 6 correspond to average basal spacings of 10.8–16 Å for the C-(N,K-)S-H products (Al/Si* = 0) and average basal spacings of 11.7–16.1 Å for the C-(N,K-)A-S-H products (Al/Si* = 0.05). In addition to the incorporation of alkali in C-(N,K-)A-S-H interlayer spaces, this variation in basal spacing is also explained by the assignment of the C-(N,K-)A-S-H products formed to poorly-ordered structural analogues of orthorhombic 14 Å tobermorite (PDF# 00-029-0331), 11 Å tobermorite (PDF# 04-017-1028), 9 Å tobermorite (PDF# 04-012-1761), a mixture of these minerals,[61] or monoclinic clinotobermorite (PDF# 01-088-1328).[59]

For the C-(N,K-)S-H samples (Al/Si* = 0), larger basal spacings are apparent in the water-synthesised specimen than in some of the alkali-containing specimens (Fig. 6A). Bach et al.[11] reported the same trend for C-(N,K-)S-H synthesised at bulk [NaOH] < 0.03 M. Here, the XRD results suggest that Na and K species are incorporated in C-(N,K-)S-H interlayers at alkali concentrations ≥0.1 M, i.e. more aqueous Na and/or K species are incorporated into interlayer spaces at higher Na and/or K content. The reduced basal spacings generally found for the samples synthesised with 0.1 M alkali hydroxide solutions relative to the water synthesised specimens can be attributed in part to exchange of interlayer Ca^{2+} with K^+ and/or Na^+

(hydrated ionic radii of Ca^{2+} = 4.12 Å, K^+ = 3.31 Å and Na^+ = 3.58 Å[64]). The comparatively large differences in basal spacings between these samples indicate that other factors, e.g. variations in the adsorbed interlayer water content, layer stacking configuration and chain lengths of the C-(N,K-)A-S-H phases formed,[59] are also likely to be important.

A clear relationship between $d_{(002)}$ and Al content is not observed in Fig. 6. However, basal spacings for Al-containing C-(N,K-)A-S-H were measured to be 2–3 Å greater than their Al-free counterparts at 20 °C,[60,62] in contrast with these results. A clear trend in $d_{(002)}$ as a function of the bulk alkali concentration is only identifiable at Ca/Si* = 0.6 for the Al-containing samples; the largest basal spacing is identified in the sample synthesised with 0.5 M NaOH/0.5 M KOH ($d_{(002)}$ = 16.1 Å). This increase is basal spacing is again explained by higher concentrations of alkali species in C-(N,K-)A-S-H interlayers at higher alkali content.

3.4 C-(N,K-)A-S-H solubility

Solubility products are calculated using eqn (5) and (6) for C-(N,K-)A-S-H with hypothetical chemical compositions of Ca/(Al + Si) = 0.6, 0.8, 1, 1.2, 1.4 and 1.6, Al/Si = 0 and 0.05, Na/(Al + Si) = 0.2 for samples containing Na, K/(Al + Si) = 0.2 for samples containing K, H_2O/Si = 1.2, and 1 mol Al + Si, and shown in Fig. 7. These Na/(Al + Si) and K/(Al + Si) ratios were chosen to approximate the alkali contents of the experimental C-(N,K-)A-S-H products (Tables 1 and 2). Hypothetical chemical compositions were chosen to enable a more direct comparison of the calculated solubility products as a function of Na, K and Al content. Solubility products for C-(N,K-)A-S-H with chemical compositions determined by mass balances from the XRD (Fig. 2), IC and pH measurements (Fig. 3), and TGA and Rietveld analysis (Appendices S3 and S4, ESI†), are shown in Appendix S6 (ESI†).

Fig. 7 shows similar values and trends in the solubility products for both the Al-free and Al-containing C-(N,K-)A-S-H end-members, i.e., the results of this study indicate that this phase is not greatly stabilised by the incorporation of Al. This is consistent with recently published results for C-(A-)S-H synthesised with Ca/Si* = 1 and cured at 7–80 °C,[14] where the measured solubility of this phase did not change greatly between Al/Si* ratios of 0 and 0.15. The downward-pointing arrows in Fig. 7 for the Ca/Si* = 0.6 and 1 C-(N,K-)A-S-H samples synthesised with 0.5 M NaOH/0.5 M KOH, and the Ca/Si* = 0.8 samples synthesised with alkali hydroxide solutions, indicate that the calculated solubility products are considered to be upper bounds; supernatant Ca concentrations were below the detection limit for these samples, so an upper limit of [Ca] = 0.004 mM was chosen. Dissolved Al concentrations were also below the detection limit for some samples (e.g. the Ca/Si* = 1.2, Al/Si* = 0.05 sample synthesised with water, Fig. 3), so [Al] = 0.003 mM was chosen for these samples. The low Al content of the C-(N,K-)A-S-H products (Al/Si ~ 0.05) means that the associated level of uncertainty in the K_s values for samples with [Al] below the detection limit is lower than for the samples with [Ca] below the detection limit;
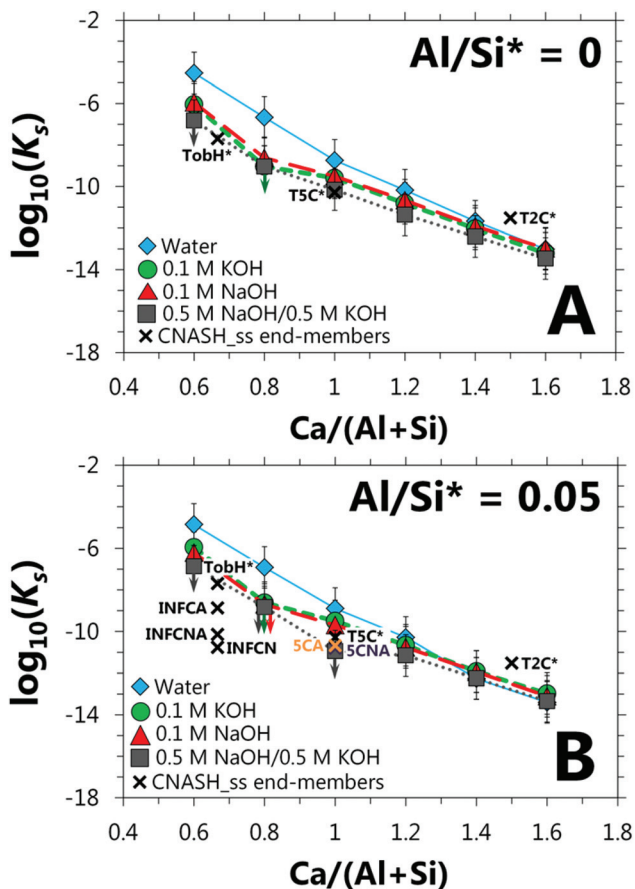
Fig. 7 Solubility products (K_s) for hypothetical C-(N,K-)A-S-H phases with chemical compositions of (A) Al/Si = 0 or (B) Al/Si = 0.05, Na/(Al + Si) = 0.2 for the Na-containing systems, K/(Al + Si) = 0.2 for the K-containing systems, H_2O/Si = 1.2, and normalised to 1 mol Al + Si at 50 °C. The estimated uncertainty depicted as error bars is ± 1 unit in the $\log_{10}(K_s)$ values, except for the points with downward-pointing arrows, which additionally represent maximum solubility product values as described in the text. The small crosses are solubility products for end-members of the CNASH_ss thermodynamic model[28] at 50 °C. Al/Si* = bulk Al/Si. Lines are for eye-guides only.

downward pointing arrows are only shown for the latter case in Fig. 7.

The lower solubility products calculated for C-(N,K-)A-S-H with higher Ca/(Al + Si) ratios in Fig. 7 reflect the increased amounts of Ca included in the stoichiometric formulae for C-(N,K-)A-S-H in these calculations at higher Ca/(Al + Si) ratios (Fig. 7 shows solubility products for C-(N,K-)A-S-H with chemical compositions normalised to one mole Al + Si), but could additionally indicate that C-(N,K-)A-S-H is stabilised at higher Ca content within the composition range analysed here. The solubility products of the C-(N,K-)A-S-H phases synthesised using 0.1 M alkali hydroxide solutions are similar irrespective of the alkali element used, indicating that both Na- and K-bearing C-(N,K-)A-S-H can be expected to form in hydrated cements with non-zero concentrations of these alkali elements. Fig. 7 also shows that C-(N,K-)A-S-H solubility generally decreases slightly as the bulk alkali hydroxide concen-

tration is increased, but this finding is only significant for some C-(N,K-)A-S-H phases with Ca/Si $\leq$ 1. Similar trends of decreasing solubility with increasing alkali content are also identified in solubility product calculations for hypothetical C-(N,K-)A-S-H phases with (Na + K)/(Al + Si) = 0 and Ca/Si $\leq$ 1, which suggests that the structure of this phase may be stabilised slightly as the bulk alkali concentration is increased. This will be discussed further in section 3.5.

The end-members of the CNASH_ss thermodynamic model (Fig. 7)[28] show the same trends in C-(N,K-)A-S-H solubility as identified experimentally here. The reduced solubilities of the Na-bearing end-members in the CNASH_ss thermodynamic model compared to the experimental results are also consistent with their much higher Na content (0.4 $\leq$ Na/(Al + Si) $\leq$ 0.46). The solubility product of the T2C* model end-member is consistent with the experimental results, although the lower solubilities of the model T5C*, TobH* and INFCA end-members relative to the experimental data indicates that their thermodynamic properties should be adjusted slightly for simulations at 50 °C to improve the temperature-dependent behaviour of CNASH_ss.

The same method of analysis presented in sections 3.1–3.4 and shown in Fig. 7 was applied to C-(N,K-)A-S-H samples with Ca/Si* = 1, Al/Si* = 0 and 0.1, and synthesised with water, 0.5 NaOH and 0.5 M NaOH/0.5 M KOH solutions. The solid and liquid phase analyses for these samples are presented in Appendix S7, ESI†, and the resulting K_s values are shown in Table 3. These data show similar trends to those described for Fig. 7, *i.e.* a slight decrease in solubility as a function of increasing alkali hydroxide concentration and no significant change in solubility as a function of the Al/Si* ratio. These results are discussed in terms of solubility–composition–structure relationships in C-(N,K-)A-S-H, using the ^{29}Si MAS NMR analysis presented for these samples, in sections 3.5–3.6 below.

3.5 ^{29}Si MAS NMR

The ^{29}Si MAS NMR spectra of the C-(N,K-)S-H samples (Al/Si* = 0) contain three resonances, that are assigned to chain-end

Table 3 Solubility products (K_s) for hypothetical C-(N,K-)A-S-H phases with chemical compositions of Ca/(Al + Si) = 1, Al/Si ratios = 0 (Al/Si* = 0) or 0.1 (Al/Si* = 0.1), Na/(Al + Si) = 0.2 for the Na-containing systems, K/(Al + Si) = 0.2 for the K-containing systems, H_2O/Si = 1.2, and normalised to 1 mol Al + Si at 50 °C. The estimated uncertainty is ± 1 unit in $\log_{10}(K_s)$ values

Al/Si* = 0	
Water	-8.7
0.5 M NaOH	-9.8
0.5 M NaOH/0.5 M KOH	-10.2
Al/Si* = 0.1	
Water	-8.9
0.5 M NaOH	-10.0
0.5 M NaOH/0.5 M KOH	$\leq -11.0^a$

^{a} Maximum values. Activities of Ca^{2+}, SiO_3^{2-}, AlO_2^-, Na^+, K^+, OH^- and H_2O were calculated using [Ca] = 0.004 mM, as the measured Ca concentration in the supernatant of this sample was below the detection limit.

sites (Q^1), bridging sites (Q^2_b) and paired sites (Q^2_p) (Fig. 8A) respectively. In the spectra of the water-synthesised samples, these resonances are described by peaks located at isotropic chemical shifts (δ_{iso}) of −79.3 ppm, −83.1 ppm and −85.1 ppm respectively. Similar δ_{iso} values have been reported for alkali- and Al-free C-S-H aged at 40 °C.[65,66] The spectrum for the Al-free sample synthesised with 0.5 M NaOH contains the same peaks but shifted by +1 to +2 ppm, which indicates that silanol groups in the 0.5 M NaOH sample are on average charge-balanced by less positively-charged species (*i.e.* Na^+ and/or H^+ rather than Ca^{2+}) relative to the alkali-free speci-men.[67] Comparable differences in δ_{iso} have also been reported between the Q^1, Q^2_b and Q^2_p sites in C-(N,K-)S-H synthesised at different alkali concentrations.[8,9] The relative intensities of the Q^1 peaks are greatly increased in the presence of NaOH and KOH, which is discussed further in the context of a reduction in mean chain length (MCL) in section 3.6 below.

^{29}Si resonances assigned to Q^1, Q^2_b and Q^2_p sites are also identified in the spectra of the C-(N,K-)A-S-H (Al/Si* = 0.1) samples (Fig. 8B). These spectra also contain an additional resonance assigned to Si in paired sites bonded to structurally-incorporated Al in bridging sites (*i.e.* Q^2(1Al)) in C-A-S-H, located at δ_{iso} = −82 ppm in the spectrum for the alkali-free sample. Q^2(1Al) sites identified in laboratory-synthesised C-A-S-H samples equilibrated at 23 °C are located at similar δ_{iso} values.[68]

Peaks assigned to Q^1, Q^2_b, Q^2_p and Q^2(1Al) are shifted by +0.4 to +1 ppm in the spectrum for the Al-containing sample synthesised with 0.5 M NaOH relative to the alkali-free C-A-S-H sample (Fig. 8B), which is consistent with ^{29}Si MAS NMR spectra of laboratory-synthesised C-(N,K-)A-S-H produced at 20–25 °C.[8,9] The intensity of the Q^1 peak is also much greater in the presence of Na and/or K in this sample, similar to the spectra for Al-free C-(N,K-)S-H (Fig. 8A). Additional Q^3(1Al) and Q^3 resonances at −88.6 and −96.8 ppm are observed in the spectrum of the 0.5 M NaOH sample, indicating the formation of a cross-linked C-(N,K-)A-S-H product. The δ_{iso} value of the Q^3 site is equivalent to the chemical shift of this site in labora-tory-synthesised C-A-S-H equilibrated at 80 °C[14] and in Al-tobermorite formed in 2000-year old Roman seawater con-crete,[31] and is similar to the chemical shift of this site in (Al-)tobermorites synthesised at 150 °C[69] and 175 °C.[70,71] However, the δ_{iso} value of the Q^3(1Al) site is shifted by approximately +3 ppm relative to the chemical shift of this site in the afore-mentioned literature; this is again attributed to the association of a greater proportion of less positively-charged dissolved species (*e.g.* Na^+ rather than Ca^{2+}) with Si atoms in Q^3(1Al) sites, resulting from the much higher alkali concentrations used here.

Each component peak is shifted to a slightly more positive δ_{iso} value by further increasing the alkali hydroxide concen-trations of the synthesis solutions to 1 M (Fig. 8B, sample 0.5 M NaOH/0.5 M KOH), suggesting additional uptake of Na^+/K^+/H^+ in C-(N,K-)A-S-H interlayers, while the Q^3 site is no longer identified. The disappearance of the Q^3 site at a bulk alkali concentration of 1 M, and the presence of Q^3(1Al) resonances at −87 to −89 ppm in the Al and alkali-containing samples, are consistent with the features of ^{29}Si MAS NMR spectra of Na_2CO_3 and Na_2SiO_3-activated slag cement pastes cured under ambient conditions,[5,72] where Q^3(1Al)-containing cross-linked C-(N,K-)A-S-H products are sometimes present in this chemical shift range. The identification of Q^3-type sites in the C-(N,K-)A-S-H samples equilibrated at 50 °C here, rather than the higher temperatures needed to form these structures in C-A-S-H specimens synthesised with Al but without alkali,[14] shows that the formation of –Al–O–Si– cross-links in C-(N,K-)A-S-H products is greatly promoted at higher alkali content. The intensity of the Q^1 peaks are further increased by increasing the alkali hydroxide concentration to 1 M.

3.6 Structural models and implications

Al/Si ratios, MCLs and cross-linked phase fractions for the C-(N,K-)A-S-H products (Fig. 9) are calculated using the ^{29}Si MAS NMR spectral deconvolution results (Fig. 8 and Appendix S8, ESI†) and the 'Cross-linked Substituted Tobermorite Model' (CSTM),[37] by representing this phase as a mixture of cross-linked and non-cross-linked tobermorite-like components.
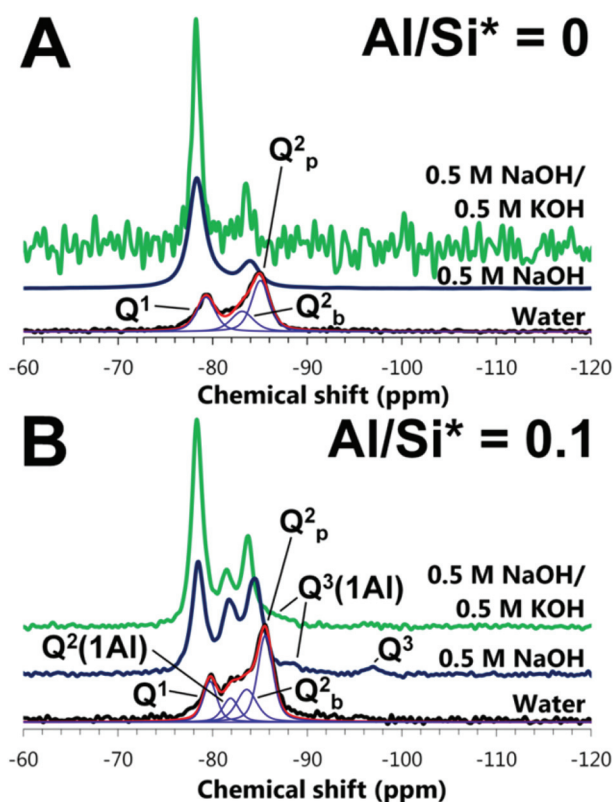
Fig. 8 Solid-state ^{29}Si MAS NMR spectra of (A) C-(N,K-)S-H (Al/Si* = 0) and (B) C-(N,K-)A-S-H (Al/Si* = 0.1) samples, synthesised with Ca/Si* = 1 and equilibrated at 50 °C. The fits and deconvoluted peaks for the spectra of the water-synthesised samples are shown as red and blue lines respectively. Deconvolutions for each spectrum are shown in Appendix S8 (ESI†). The relatively high level of noise in the spectrum of the Al/Si* = 0 sample synthesised with 0.5 M NaOH/0.5 M KOH is caused by the very rapid relaxation of this sample. Al/Si* = bulk Al/Si.
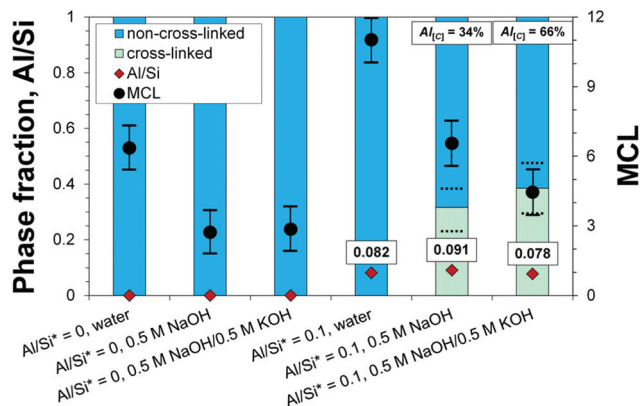
Fig. 9 C-(N,K-)S-H and C-(N,K-)A-S-H structural parameters calculated from deconvolution analysis of the ^{29}Si MAS NMR spectra (Fig. 8), determined using the 'Cross-linked Substituted Tobermorite Model' (CSTM)[37] for mixed cross-linked/non-cross-linked tobermorite-like phases. The expected error bounds of the deconvolution results are represented by symbol size for the Al/Si ratios, by dotted black lines for the cross-linked phase fractions and by error bars for the MCL values. $Al_{[C]}$ = percentage of Al in cross-linked C-(N,K-)A-S-H (eqn (1)). Al/Si* = bulk Al/Si.

The results obtained by applying the CSTM[37] to the ^{29}Si MAS NMR spectral deconvolutions show that the MCLs of the C-(N,K-)A-S-H products decrease with increasing alkali concentration, due mainly to the much greater prevalence of Q^1 sites in the presence of Na and/or K (Fig. 8). The calculated MCLs are also lower in the systems containing less Al. The calculated Al/Si ratios are similar to the Al/Si* ratios used in synthesis (Al/Si* = 0.1), with the small differences explained by the formation of small amounts of $C_3AH_6/Al(OH)_3$ in the alkali-free and 0.5 M NaOH/0.5 M KOH samples, and $C_4AcH_{11}/C_3AH_6/Al(OH)_3$ in the 0.5 M NaOH sample (Appendix S7, ESI†).[14] The alkali and Al-containing C-(N,K-)A-S-H products show similar levels of cross-linking, although the percentage of Al in the cross-linked components ($Al_{[C]}$) of this phase is higher in the sample synthesised using 0.5 M NaOH/0.5 M KOH (66%) relative to the sample synthesised with 0.5 M NaOH (34%).

The calculated $Al_{[C]}$ values (Fig. 9) show that the uptake of Al into cross-linked C-(N,K-)A-S-H components is enhanced as the bulk alkali hydroxide concentration is increased, but also that there is not an extremely strong preference for partitioning of Al into either one of the two structural types. This view is supported by recent work on the role of Al in cross-linking of C-(N,K-)A-S-H in Na_2SiO_3-activated slag cements cured for 1–180 days at room temperature, which reported $Al_{[C]}$ values of 40–60%.[72]

The key alkali-dependent structural changes are therefore: reduced MCL (Fig. 9); increased basal spacings at Ca/Si* ratios <1 (Fig. 6); and increased cross-linking and $Al_{[C]}$ (in the presence of Al, Fig. 9) at higher alkali hydroxide concentrations. A comparison of these structural changes with the slightly reduced C-(N,K-)A-S-H solubilities determined at higher alkali hydroxide concentration and Ca/(Al + Si) ratios ≤1 (section 3.4) suggests that the solubility and MCL of this phase may be

directly related in this range of Ca/(Al + Si) ratios. The influence of Ca composition on C-(N,K-)A-S-H solubility dominates at higher Ca/(Al + Si) ratios, *i.e.* at low MCL values, demonstrated by large reductions in the solubility of this phase as a function of increasing Ca/(Al + Si) ratio at the limit MCL → 2 (region A in Fig. 10). The Ca/Si ratios obtained by mass balance and marked in the legend in Fig. 10 reflect the total amount of Ca in C-(N,K-)A-S-H; this parameter does not distinguish between Ca present as charge-balancing cations in the interlayer or adsorbed on external surfaces, or structurally-bound in Ca–O sheets (Fig. 1), whereas the MCL parameter describes the structure of the (alumino)silicate chains and Ca–O sheets only.

The effects of MCL and Ca/(Al + Si) ratio on C-(N,K-)A-S-H solubility cannot be distinguished from one another in region B of Fig. 10 because C-(N,K-)A-S-H can contain many different total Ca/(Al + Si) ratios at a fixed MCL value, for MCL > 5.[59] Therefore, selected solubility data for C-(N,K-)A-S-H with Ca/(Al + Si) = 1 were plotted as a function of MCL in Fig. 11.

Fig. 11 shows an inverse correlation between MCL and the bulk alkali hydroxide concentration, in good agreement with the ^{29}Si MAS NMR results presented in Fig. 9, and also slightly reduced C-(N,K-)A-S-H solubility products in samples synthesised with more highly concentrated alkali hydroxide solutions, consistent with the trends in C-(N,K-)A-S-H solubility
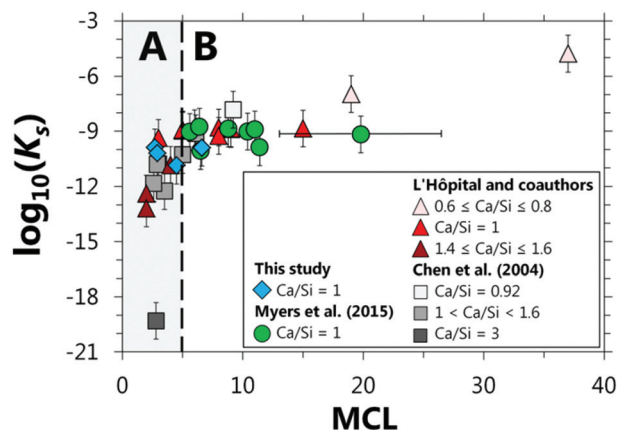
Fig. 10 Solubility products for C-(N,K-)A-S-H plotted as a function of MCL, calculated using the dissolution reaction shown in eqn (5) with regions: (A) describing C-(N,K-)A-S-H with highly variable Ca/(Al + Si) ratios and slightly variable MCL; and (B) describing C-(N,K-)A-S-H with variable Ca/(Al + Si) and MCL. The references for the symbols used are: blue diamonds, this study; green circles, C-(A-)S-H equilibrated at 7–80 °C in ref. 14; red triangles, C-(N,K-)A-S-H equilibrated at 20 °C in ref. 8 and 60; and grey squares, C-S-H equilibrated at 22 °C in ref. 73. Solubility products are calculated using H_2O/Si = 1.2 and Ca/Si ratios taken directly from the literature for the data in ref. 73, or specified to have a total of 1 mole Si + Al with Ca/Si and Al/Si ratios equivalent to the bulk Ca-Al-Si compositions used, Na/Si ratios = 0.2 for the Na-containing phases, K/Si ratios = 0.2 for the K-containing phases and H_2O/Si ratios = 1.2 for the data in ref. 8, 14 and 60 and in this study. The expected experimental uncertainty is represented by error bars, or by the size of the symbols used in the absence of horizontal error bars for MCL values.
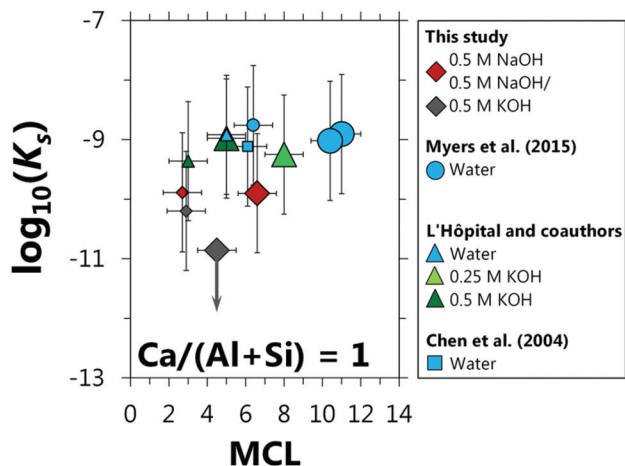
Fig. 11 Solubility products for C-(N,K-)A-S-H plotted as a function of the MCL, calculated using the dissolution reaction shown in eqn (5) at a Ca/(Al + Si) ratio = 1. The references for the symbols used are: diamonds, this study (Ca/Si* = 1); circles, C-(A-)S-H synthesised with Ca/Si* = 1 and equilibrated at 20–50 °C in ref. 14; triangles, C-(N,K-)A-S-H synthesised with Ca/Si* = 1 and equilibrated at 20 °C in ref. 8 and 60; and square, C-S-H equilibrated at 22 °C with Ca/Si = 1.03 in ref. 73. Large symbols are data at Al/Si* = 0.1 and small symbols are data at Al/Si* = 0. C-(N,K-)A-S-H solubility products are calculated using H_2O/Si = 1.2 and Ca/Si ratios taken directly from the literature for the datum in ref. 73, or specified to have a total of 1 mole Si + Al with Ca/Si and Al/Si ratios equivalent to the bulk Ca-Al-Si compositions used, Na/Si ratios = 0.2 for the Na-containing phases, K/Si ratios = 0.2 for the K-containing phases and H_2O/Si ratios = 1.2 for the data in ref. 8, 14 and 60 and in this study. Error bars represent the expected experimental uncertainty except for the point with a downward-pointing arrow, which additionally represents a maximum solubility product value, as described in the text for Fig. 7.

shown in Fig. 7 at Ca/(Al + Si) = 1. However, Fig. 11 does not show a significant difference in C-(N,K-)A-S-H solubility as a function of Al content, despite the longer chain lengths of the Al-containing C-(N,K-)A-S-H phases compared to their Al-free counterparts. Therefore, these results indicate that the MCL structural parameter does not play a key role in influencing the solubility of C-(N,K-)A-S-H at a Ca/(Al + Si) ratio = 1. This analysis is consistent with recently reported results for C-(A-)S-H that showed comparable solubility products for this phase independent of the Al content.[14]

Alternative factors that could account for the slightly stabilised C-(N,K-)A-S-H structures identified here at increased bulk alkali hydroxide concentrations and Ca/(Al + Si) ratios ≤1 (Fig. 7) would then need to be proposed: increased cross-linking (Fig. 9) or changes to the nanoparticulate layered structure of this phase (Fig. 6 and ref. 59) could be potential candidates. However, the large uncertainty (±1 log_{10} unit) of the solubility products calculated here (Fig. 7) and the limited availability of solubility data for C-(N,K-)A-S-H at Ca/(Al + Si) ratios <1 mean that these proposed structure–solubility relationships cannot be considered fully conclusive. Further work clarifying the role of structure on the solubility of C-(N,K-)-A-S-H would be greatly beneficial in further enabling the

design of chemically-stable and durable cementitious binders based on engineering controls such as the mix design and curing temperature.

4. Conclusions

The effect of alkali, Al and Ca on the structure and solubility of C-(N,K-)A-S-H equilibrated at 50 °C was investigated in this paper. In general, similar composition–solubility–structure trends are observed at 20 °C to those identified here. The long-range order of the alkali-containing C-(N,K-)A-S-H products was much greater than in those synthesised in the absence of alkalis. C-(N,K-)A-S-H basal spacings were generally greater at lower Ca content and at higher alkali concentrations in the samples synthesised using alkaline hydroxide solutions; this latter factor was attributed to the uptake of additional Na^+/K^+ species in C-(N,K-)A-S-H interlayers. However, no clear trend in basal spacing as a function of Al content was identified here, in contrast to results reported for this phase at 20 °C.

The concentrations of Ca decreased and the concentrations of Si and Al increased in the supernatants as functions of increasing alkali hydroxide concentration. More alkali was incorporated in C-(N,K-)A-S-H synthesised with lower Ca and higher alkali hydroxide concentrations. Alkali uptake in this phase was found to be independent, within the experimental uncertainty, of the alkali type (Na or K) and Al/Si ratio at the relatively low amounts of Al added to each sample (bulk Al/Si ≤ 0.05).

Shorter mean chain lengths, increased cross-linking, and incorporation of more Al into cross-linked C-(N,K-)A-S-H components were identified upon increasing the bulk alkali and Al content. Mixed cross-linked/non-cross-linked C-(N,K-)A-S-H was only formed in the presence of both alkali and Al. A reduction in C-(N,K-)A-S-H solubility was found at higher bulk alkali hydroxide concentrations, but this result was only significant for some samples prepared with bulk Ca/Si ratios ≤1. The stability of this phase did not vary greatly as a function of the Al/Si ratio. The reduced C-(N,K-)A-S-H solubility calculated at higher alkali content was discussed to be partly related to structural changes in this phase, and it was tentatively proposed that the MCL does not play a key role in these solubility–structure relationships. These results provide new insight into the composition–structure–solubility relationships in C-(N,K-)A-S-H, which will improve how hydrated alkali and Al-containing cements are understood to perform in service.

Acknowledgements

E. L'Hôpital. The NMR hardware was partially granted by the Swiss National Science Foundation (grant 206021_150638/1).

References

1 H. F. W. Taylor, *Cement Chemistry*, Thomas Telford Publishing, London, 1997.

2 A. Fernández-Jiménez and A. Palomo, *Fuel*, 2003, **82**, 2259–2265.

3 J. L. Provis and S. A. Bernal, *Annu. Rev. Mater. Res.*, 2014, **44**, 299–327.

4 R. Snellings, *J. Am. Ceram. Soc.*, 2013, **96**, 2467–2475.

5 S. A. Bernal, J. L. Provis, R. J. Myers, R. San Nicolas and J. S. J. van Deventer, *Mater. Struct.*, 2015, **48**, 517–529.

6 T. Chappex and K. Scrivener, *Cem. Concr. Res.*, 2012, **42**, 1049–1054.

7 A. Leemann, G. Le Saout, F. Winnefeld, D. Rentsch and B. Lothenbach, *J. Am. Ceram. Soc.*, 2011, **94**, 1243–1249.

8 E. L'Hôpital, B. Lothenbach, G. Le Saoût, D. A. Kulik and K. Scrivener, *Cem. Concr. Res.*, 2015, **75**, 91–103.

9 I. Lognot, I. Klur and A. Nonat, in *Nuclear magnetic resonance spectroscopy of cement-based materials*, ed. P. Colombet, H. Zanni, A.-R. Grimmer and P. Sozzani, Springer, Berlin, 1998, ch. 13, pp. 189–196.

10 J. Duchesne and E. J. Reardon, *Cem. Concr. Res.*, 1995, **25**, 1043–1053.

11 T. T. H. Bach, E. Chabas, I. Pochard, C. Cau-dit-Coumes, J. Haas, F. Frizon and A. Nonat, *Cem. Concr. Res.*, 2013, **51**, 14–21.

12 I. G. Richardson and G. W. Groves, *J. Mater. Sci.*, 1993, **28**, 265–277.

13 I. G. Richardson, *Cem. Concr. Res.*, 2008, **38**, 137–158.

14 R. J. Myers, E. L'Hôpital, J. L. Provis and B. Lothenbach, *Cem. Concr. Res.*, 2015, **68**, 83–93.

15 L. Pegado, C. Labbez and S. V. Churakov, *J. Mater. Chem. A*, 2014, **2**, 3477–3483.

16 M. D. Andersen, H. J. Jakobsen and J. Skibsted, *Cem. Concr. Res.*, 2006, **36**, 3–17.

17 G. Renaudin, J. Russias, F. Leroux, C. Cau dit Coumes and F. Frizon, *J. Solid State Chem.*, 2009, **182**, 3320–3329.

18 G. K. Sun, J. F. Young and R. J. Kirkpatrick, *Cem. Concr. Res.*, 2006, **36**, 18–29.

19 C. Labbez, I. Pochard, B. Jönsson and A. Nonat, *Cem. Concr. Res.*, 2011, **41**, 161–168.

20 E. Bonaccorsi, S. Merlino and A. R. Kampf, *J. Am. Ceram. Soc.*, 2005, **88**, 505–512.

21 S. Y. Hong and F. P. Glasser, *Cem. Concr. Res.*, 1999, **29**, 1893–1903.

22 D. E. Macphee, K. Luke, F. P. Glasser and E. E. Lachowski, *J. Am. Ceram. Soc.*, 1989, **72**, 646–654.

23 G. L. Kalousek, *J. Res. Natl. Bur. Stand.*, 1944, **32**, 285–302.

24 S. J. Way and A. Shayan, *Cem. Concr. Res.*, 1992, **22**, 915–926.

25 H. Stade, *Cem. Concr. Res.*, 1989, **19**, 802–810.

26 P. Nieto and H. Zanni, *J. Mater. Sci.*, 1997, **32**, 3419–3425.

27 B. Lothenbach, G. Le Saout, M. Ben Haha, R. Figi and E. Wieland, *Cem. Concr. Res.*, 2012, **42**, 410–423.

28 R. J. Myers, S. A. Bernal and J. L. Provis, *Cem. Concr. Res.*, 2014, **66**, 27–47.

29 B. Lothenbach, K. Scrivener and R. D. Hooton, *Cem. Concr. Res.*, 2011, **41**, 1244–1256.

30 R. Taylor, I. G. Richardson and R. M. D. Brydson, *Cem. Concr. Res.*, 2010, **40**, 971–983.

31 M. D. Jackson, S. R. Chae, S. R. Mulcahy, C. Meral, R. Taylor, P. Li, A.-H. Emwas, J. Moon, S. Yoon, G. Vola, H.-R. Wenk and P. J. M. Monteiro, *Am. Mineral.*, 2013, **98**, 1669–1687.

32 H. Viallis, P. Faucon, J. C. Petit and A. Nonat, *J. Phys. Chem. B*, 1999, **103**, 5212–5219.

33 J. Skibsted and M. D. Andersen, *J. Am. Ceram. Soc.*, 2013, **96**, 651–656.

34 S. Y. Hong and F. P. Glasser, *Cem. Concr. Res.*, 2002, **32**, 1101–1111.

35 E. L'Hôpital, B. Lothenbach, K. Scrivener and D. A. Kulik, *Cem. Concr. Res.*, submitted.

36 B. H. O'Connor and M. D. Raven, *Powder Diffr.*, 1988, **3**, 2–6.

37 R. J. Myers, S. A. Bernal, R. San Nicolas and J. L. Provis, *Langmuir*, 2013, **29**, 5294–5306.

38 D. A. Kulik, T. Wagner, S. V. Dmytrieva, G. Kosakowski, F. F. Hingerl, K. V. Chudnenko and U. Berner, *Comput. Geosci.*, 2013, **17**, 1–24.

39 T. Wagner, D. A. Kulik, F. F. Hingerl and S. V. Dmytrieva, *Can. Mineral.*, 2012, **50**, 1173–1195.

40 T. Thoenen, W. Hummel and U. Berner, *Mineral. Mag.*, 2013, **77**, 2327.

41 W. Hummel, U. Berner, E. Curti, F. J. Pearson and T. Thoenen, *Nagra/PSI Chemical Thermodynamic Database 01/01*, Universal Publishers, Parkland, Florida, 2002.

42 D. A. Kulik and M. Kersten, *J. Am. Ceram. Soc.*, 2001, **84**, 3017–3026.

43 B. Lothenbach, T. Matschei, G. Möschner and F. P. Glasser, *Cem. Concr. Res.*, 2008, **38**, 1–18.

44 B. Lothenbach and F. Winnefeld, *Cem. Concr. Res.*, 2006, **36**, 209–226.

45 T. Matschei, B. Lothenbach and F. P. Glasser, *Cem. Concr. Res.*, 2007, **37**, 1379–1410.

46 G. Möschner, B. Lothenbach, J. Rose, A. Ulrich, R. Figi and R. Kretzschmar, *Geochim. Cosmochim. Acta*, 2008, **72**, 1–18.

47 G. Möschner, B. Lothenbach, F. Winnefeld, A. Ulrich, R. Figi and R. Kretzschmar, *Cem. Concr. Res.*, 2009, **39**, 482–489.

48 T. Schmidt, B. Lothenbach, M. Romer, K. Scrivener, D. Rentsch and R. Figi, *Cem. Concr. Res.*, 2008, **38**, 337–349.

49 D. A. Kulik and M. Kersten, *Environ. Sci. Technol.*, 2002, **36**, 2926–2931.

50 B. Lothenbach, L. Pelletier-Chaignat and F. Winnefeld, *Cem. Concr. Res.*, 2012, **42**, 1621–1634.

51 B. Z. Dilnesa, B. Lothenbach, G. Renaudin, A. Wichser and D. Kulik, *Cem. Concr. Res.*, 2014, **59**, 96–111.

52 H. C. Helgeson, D. H. Kirkham and G. C. Flowers, *Am. J. Sci.*, 1981, **281**, 1249–1516.

53 Y. Lee, Y. Lee and D. Seoung, *Am. Mineral.*, 2010, **95**, 1636–1641.

54 T. Runčevski, R. E. Dinnebier, O. V. Magdysyuk and H. Pöllmann, *Acta Crystallogr., Sect. B: Struct. Sci.*, 2012, **68**, 493–500.

55 P. Faucon, J. C. Petit, T. Charpentier, J. F. Jacquinot and F. Adenot, *J. Am. Ceram. Soc.*, 1999, **82**, 1307–1312.

56 X. Pardal, I. Pochard and A. Nonat, *Cem. Concr. Res.*, 2009, **39**, 637–643.

57 H. M. Jennings, *Cem. Concr. Res.*, 2008, **38**, 275–289.

58 A. C. A. Muller, K. L. Scrivener, A. M. Gajewicz and P. J. McDonald, *Microporous Mesoporous Mater.*, 2013, **178**, 99–103.

59 I. Richardson, *Acta Crystallogr., Sect. B: Struct. Sci.*, 2014, **70**, 903–923.

60 E. L'Hôpital, PhD thesis, École Polytechnique Fédérale de Lausanne, 2014.

61 S. Grangeon, F. Claret, Y. Linard and C. Chiaberge, *Acta Crystallogr., Sect. B: Struct. Sci.*, 2013, **69**, 465–473.

62 G. Renaudin, J. Russias, F. Leroux, F. Frizon and C. Cau dit Coumes, *J. Solid State Chem.*, 2009, **182**, 3312–3319.

63 K. Garbev, G. Beuchle, M. Bornefeld, L. Black and P. Stemmermann, *J. Am. Ceram. Soc.*, 2008, **91**, 3005–3014.

64 B. E. Conway, *Ionic hydration in chemistry and biophysics*, Elsevier Scientific, Amsterdam, 1981.

65 X. Cong and R. J. Kirkpatrick, *Adv. Cem. Based Mater.*, 1996, **3**, 144–156.

66 F. Brunet, P. Bertani, T. Charpentier, A. Nonat and J. Virlet, *J. Phys. Chem. B*, 2004, **108**, 15494–15502.

67 P. Rejmak, J. S. Dolado, M. J. Stott and A. Ayuela, *J. Phys. Chem. C*, 2012, **116**, 9755–9761.

68 X. Pardal, F. Brunet, T. Charpentier, I. Pochard and A. Nonat, *Inorg. Chem.*, 2012, **51**, 1827–1836.

69 J. Houston, R. Maxwell and S. Carroll, *Geochem. Trans.*, 2009, **10**, 1–14.

70 M. Tsuji, S. Komarneni and P. Malla, *J. Am. Ceram. Soc.*, 1991, **74**, 274–279.

71 X. Cong and R. J. Kirkpatrick, *Adv. Cem. Based Mater.*, 1996, **3**, 133–143.

72 R. J. Myers, S. A. Bernal, J. L. Provis, J. D. Gehman and J. S. J. van Deventer, *J. Am. Ceram. Soc.*, 2015, **98**, 996–1004.

73 J. J. Chen, J. J. Thomas, H. F. W. Taylor and H. M. Jennings, *Cem. Concr. Res.*, 2004, **34**, 1499–1519.